Scripta Scientifica Medica, 2022;54(3):27-33
DOI: 10.14748/ssm.v54i2.8361

ISSN 0582-3250 (Print)
ISSN 1314-6408 (Online)

ORIGINAL ARTICLES

# DESIGN AND USE OF COMPUTATIONAL MODELS FOR CONTRAST-ENHANCED SPECTRAL MAMMOGRAPHY

**Yanka Baneva[1], Tihomir Georgiev[2], Kristina Bliznakova[2]**

*[1]Department of Physics and Biophysics, Faculty of Pharmacy, Medical University of Varna*
*[2]Department of Medical Equipment, Electronic and Information Technologies in Healthcare, Faculty of Public Health, Medical University of Varna*

## ABSTRACT

**INTRODUCTION: Contrast-enhanced spectral mammography (CESM) is a new technique for cancer investigations. The application of this technique to screen the breast would result in contrast improvement of the different breast lesions. This can be effectively ensured by the use of phantoms. Computational phantoms are one of the ways to investigate the characteristics of the received image and thus to evaluate the whole technique.**

**AIM: The aim of this study is to validate and analyse the design of three different computational phantoms for CESM.**

**MATERIALS AND METHODS: An in-house software tool was used to create three computational phantoms, consisting of iodinated inserts for the simulation of the CESM procedure. The inserts in the phantoms, modelled from Omnipaque, have a radius of 8–10 mm and varying height. The three phantoms are made of polymethyl methacrylate (PMMA), with different shape and composition. One of the phantoms is characterised by a heterogeneous background. For each phantom two x-ray radiographs were generated, one at x-ray energy of 20keV and one at 34 keV. The images were processed to obtain a recombined iodine image, which shows the iodine contrast agent and suppresses the surrounding background tissue.**

**RESULTS: Simulated spectral images demonstrated a great improvement of the image quality compared to low-energy images of the phantoms. The simulations with the inhomogeneous model revealed that the heterogeneous background has been successively depressed while improving the visibility of the iodine inserts.**

**CONCLUSION: The heterogeneous breast phantom might be used as a reference tool for information about the needed iodine concentration which needs to be inserted during the procedure to obtain significant enhancement in the suspicious area.**

**Keywords:** *computational breast models, contrast-enhanced spectral mammography, iodine concentration, modelling, simulation*

**Address for correspondence:**
*Kristina Bliznakova*
*Faculty of Public Health*
*Medical University of Varna*
*55 Marin Drinov St*
*9002 Varna*
*e-mail: Kristina.Bliznakova@mu-varna.bg*

**Received**: August 11, 2022
**Accepted**: October 2, 2022

## INTRODUCTION

Small cancerous lesions are difficult to detect in women with dense breasts. The overlap of diagnostic relevant tissue structures in women with dense breasts and the applied dose that is limited due to the radiation susceptibility of the breast are some of the main issues in breast imaging (1). A new technology for early detection of breast cancer is the contrast-enhanced spectral mammography (CESM), a novel

technique based on dual-energy acquisitions after injection of iodine-based contrast media. Two x-ray images are obtained at two different x-ray energies in respect to the K-edge of the contrast inserted material and hypervascularized breast lesions are expected to be seen on the recombined images (2). At present, there are no standardized interpretation criteria for the evaluation of breast lesions on CESM (3). Some authors suggest that intensity and pattern of enhancement on CESM might bring (together with the results of diagnostic imaging methods) not only the confirmation of presence or absence of a tumour, but also prognostic information (4).

Optimisation of this technique is closely related to the use of suitable physical phantoms, which are also used to perform daily quality control of CESM devices. Designs of these specific phantoms varies. They may be modular, composed of two types of step blocks – a breast with iodine contrast block, and adipose-glandular density blocks. Such modularity allows combinations of blocks to be arranged to represent the compressed breast for small to large patients (5). Another physical phantom for CESM is the CIRS CESM phantom. It consists of four slabs. A target slab is made from 50/50 ratio of gland and adipose breast-equivalent tissue material. The slab contains two sets of four plugs, each plug having different iodine concentration and another fifth plug is made of 100% glandular tissue-equivalent material. This plug is positioned in the centre of each plug group to mimic a glandular lesion. The contrast slab consists of half 100% adipose material and half 100% glandular material to test iodine separation from the background over a wide range of densities. The top and bottom slabs are made from 100% adipose material and have rounded edges to mimic the realistic shape of a compressed breast (6). Another in-house developed phantom is the three-dimensional phantom, proposed by Baldelli *et al.* (7). The phantom consists of a 5 cm thick polymethyl methacrylate (PMMA) box, filled with animal fat for simulating adipose tissue and PMMA spheres of two different diameters, 8 and 12.7 mm, respectively, for simulating fibroglandular tissue. A 1 cm thick PMMA slab containing cavities with two different diameters (5 and 8 mm) is placed in the middle of the box. Cavities are then filled with different solutions of water and Ultravist. Similarly, Contillo *et al.* (8), proposed a phantom, designed as a box of parallelepipedal shape, made of PMMA and filled with a large number of PMMA spheres of different diameters, embedded in a paraffin wax. Moreover, it embeds a system of cavities that can be filled with iodine solutions of various concentrations.

## AIM

The design, optimisation and validation of physical phantoms dedicated to specific radiological tasks require both materials and time. Phantoms and more specifically computational phantoms may assist us to explore and test novel ideas before developing the physical phantom with the established from the simulations optimised parameters. The aim of this study is to design different in complexity computational CESM phantoms, to investigate objectively and subjectively the visibility of iodine inserts in the CESM images and decide which is appropriate for physical manufacturing.

## MATERIALS AND METHODS

### *Design of the Phantoms with Contrast Agent*

Three computational phantoms were designed with the in-house developed software tool *XRAY-ImagingSimulator* (9). This software application has three main modules: (a) a module for creation of 3D objects, (b) a module to generate x-ray images from 3D objects and simulated geometry, and (c) a module to visualize 3D objects and x-ray images. One of the possibilities to create 3D objects is by combination of 3D geometrical primitives, which are spheres, ellipsoids, cylinders, parallelepipeds. This possibility is used for the construction of the three computational phantoms shown in Fig. 1 along with their description. Every object has an elemental composition, dimensions, and position.

### *Generating of Planar Images*

For each phantom, two simulated radiographs were computationally generated: one at energy of 20 keV and one at higher energy – 34 keV. These images were synthesized with the second module of the *XRAYImagingSimulator*. The modelled geometry is shown in Fig. 2, where the x-ray tube and detector were modelled to be at a distance D1 and D2 equal to 603 mm and 660 mm, respectively.

The simulated x-ray projection images of the computational phantoms were modelled with a pixel

| Phantom | Description |
|---|---|
| 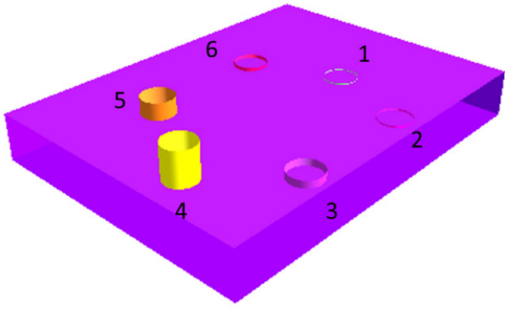 Phantom 1 | The first phantom is a PMMA parallelepiped with dimensions of 203 mm x 152 mm x 25 mm (length x width x thickness). Six Omnipaque cylinders with radii of 9.5 mm and varying heights from 0.5 mm to 20 mm are placed inside the PMMA box. |
| 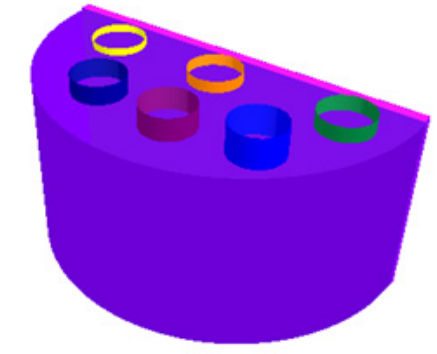 Phantom 2 | The second phantom is a semicylinder with a radius of 50 mm and a height of 45 mm, with assigned PMMA composition.<br>Six Omnipaque cylinders with radii of 10 mm and height of 2–8 mm are placed inside the PMMA semicylinder. |
| 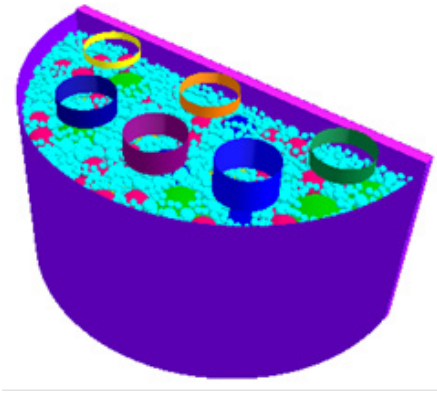 Phantom 3 | The third phantom was designed as a heterogenous breast phantom. The phantom is made of PMMA semicylinder with a radius of 50 mm, and a height of 48 mm. Six Omnipaque cylinders with radii of 8 mm and height of 0.1–0.6 mm are placed in the PMMA semicylinder. Heterogeneity is achieved by the creation of heterogeneous background using more than 8000 spheres of different radius, which varies between 0.79 mm and 7.94 mm. |

*Fig. 1. Description of the designed computational phantoms.*

size of 100 μm. Modelling of detector noise was not concerned in this simulation study. The final intensity images were based on the Beer's law:

$$I = I_0 * \exp\left( -\int_{ll} \mu(x,y,z)dl \right) \quad (1)$$

where μ(x,y,z) is the spatially dependent linear attenuation coefficient, l is the path length through the object and $I_0$ is the intensity of radiation at the source segment that emits to the area of the detector, taken equal for all viewing angles.

### *Generating CESM Images*

Energies were selected respectively below and above the iodine K-edge, which is at 32.17 keV. The

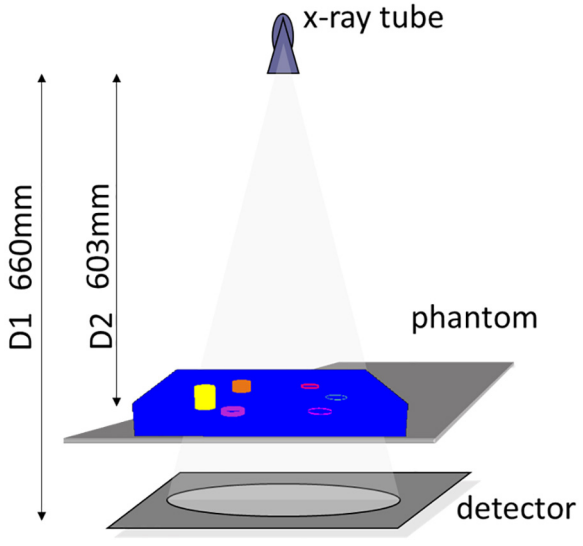


*Fig. 2. Simulated x-ray imaging geometry used in the synthesis of x-ray images from the computational CESM phantoms.*

images were processed with the aim of creating a resulting image, called recombined CESM image, which visually intensifies the contrast by suppressing the surrounding background tissue. This concept of using two different energies is exploited to obtain better visualization for specific tissues. X-ray images are acquired at different diagnostics x-ray energies and then these primary images are processed by using weighted subtraction, which results in removal of a given tissue type in the recombined image. In this study, the low and high energy images were subtracted in order to remove the phantoms' background and increase the visibility of iodine inserts. The assumption made was that the breast was composed of three different tissue components: glandular, adipose, and cancerous. To further simplify the modelling task, we assumed that the adipose and the glandular tissues would be represented as one combined tissue with equivalent adipose-glandular weighted contribution and thus to design the breast structures by only two components: breast tissue and calcifications. This is reflected in Fig. 3, where the compressed breast is composed of breast tissue with a thickness of *l*, while the breast lesion is with a thickness *c* (10).

Using the CESM technique, the visibility of the normal breast tissues was expected to be reduced, thus enhancing the contrast of the breast lesion. Further, the recombined image was calculated as follows:

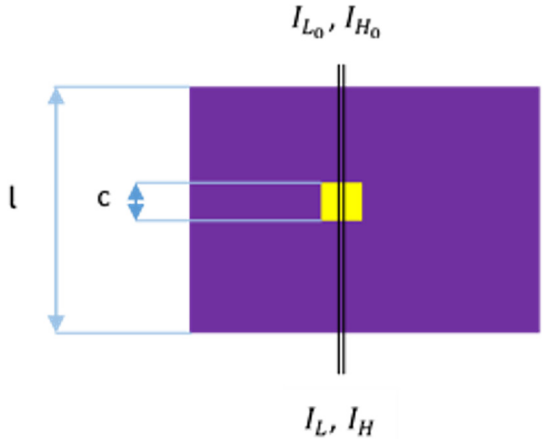


*Fig. 3. Simplified representation of compressed breast with a single breast lesion. The large square represents the compressed breast, the small square represents the breast lesion, $I_{Lo}$, $I_{Ho}$, $I_L$, and $I_H$, respectively, are the low and the high energy intensity at the detector and* l *and c are the thicknesses of the compressed breast and of the lesion.*

$$I_R = I_L - \frac{\mu_{LT}}{\mu_{HT}} I_H \quad (2)$$

where is the calculated intensity, while and are the attenuation coefficients of the phantom's background at the low and high energy. All operations were pixel-based.

### *Evaluation of the Used Method*

The evaluation of the designed computational phantoms was implemented subjectively by assessing the visibility of the inserts in the recombined images and objectively, by calculation of the subject contrast of these inserts. For this purpose, two types of regions of interest (ROI) were assigned for each simulated low energy and recombined image. Specifically, the first type of ROI was referred to as $ROI_{object}$ and was positioned within the areas of the contrast agent insert, while the second type of ROI was referred to as $ROI_{back}$ and was positioned in the background area. All ROI were 60 pixels x 60 pixels, corresponding to an area of 36 mm$^2$. The average values of the pairing ROIs were taken for further calculations as follows:

$$C = \frac{R_{object} - R_{back}}{R_{back}} \quad (3)$$

## RESULTS

Fig. 4a and Fig. 4b show the simulated planar x-ray projections of phantom 1 for energies 20 keV and 34 keV respectively, while the recombined CESM images, obtained as a result of applying the subtraction algorithm are shown in Fig. 4c.

Table 1 summarizes the contrast calculations for the three computational phantoms.

The improvement in contrast in the CESM image compared to the low-energy image is shown in Fig. 5.

## DISCUSSION

The contrast inserts in the first phantom were cylinders with varying height (from 0.5 mm to 20 mm) and a constant diameter of 19 mm. These cylinders were filled with Omnipaque, used in diagnostic procedures where contrast enhancement is required. The visual comparison of objects between the recombined and low-energy image (Fig. 4, first row) showed that the visibility of cylinders with higher thickness was increased, however, the visibility of the thinner objects was also well improved. As seen from Fig. 4a (first row), the cylinder that is 0.5 mm thick (ROI 1 of the simulated low x-ray energy image), is barely noticeable but this omnipaque object is well visible in the recombined CESM image (Fig. 4c, first row). This result was also well supported by the objective evaluation of the contrast in low-energy and recombined images, showing approximately 129-fold amplification of the contrast values for the contrast-enhanced image (Fig. 5). The same contrast improvement was observable as well for the rest of the iodine cylinders. This was due to that fact that this phantom was characterised by a homogeneous background,

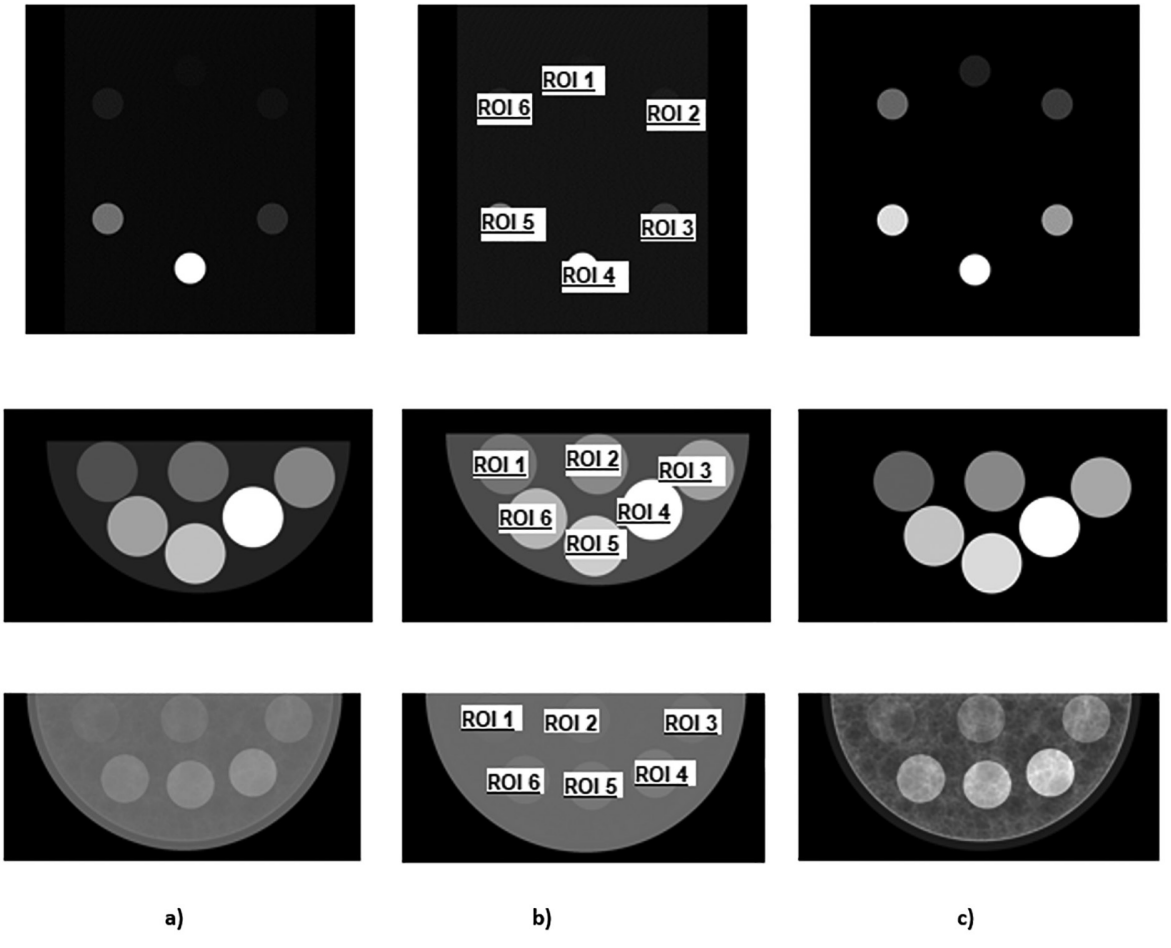


*Fig. 4. Planar x-ray images of the computational phantoms dedicated a) at x-ray energy 20 keV, b) at x-ray energy 34 keV, c) recombined CESM image.*

*Table 1. Objects'contrast evaluation*

| | ROI1 | ROI2 | ROI3 | ROI4 | ROI5 | ROI6 |
|---|---|---|---|---|---|---|
| Phantom 1 contrast at 20 keV | 0.47 | 0.95 | 3.79 | 1.89 | 18.93 | 9.47 |
| Phantom 1 recombined contrast | 60.50 | 120.99 | 483.97 | 241.99 | 2419.87 | 1209.94 |
| Phantom 2 contrast at 20 keV | 1.023 | 1.54 | 2.05 | 2.56 | 3.07 | 4.09 |
| Phantom 2 recombined contrast | 130.64 | 195.96 | 261.28 | 326.60 | 391.92 | 522.56 |
| Phantom 3 contrast at 20 keV | 0.04 | 0.09 | 0.14 | 0.17 | 0.22 | 0.27 |
| Phantom 3 recombined contrast | 0.69 | 0.48 | 0.65 | 0.79 | 0.99 | 1.28 |

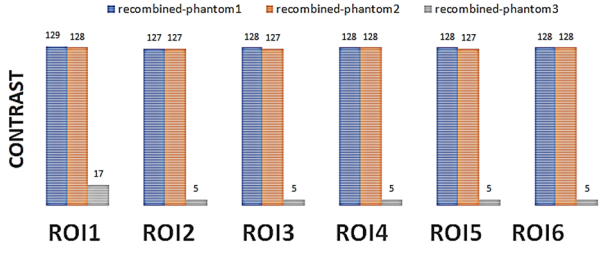


*Fig. 5. The improvement of the contrast in the different ROIs for the recombined phantoms images.*

i.e., the PMMA parallelepiped, whose influence was subtracted as a result of the subtraction algorithm.

The second phantom represented a breast in a compressed form (Fig. 4c, second row). Visually, the contrast of all contrast inserts was very well enhanced in the CESM image, which was due both to the subtraction algorithm and the relatively large, simulated area of the objects (20 mm in diameter). Similarly, the objective evaluation in Fig. 5 showed approximately a 127-fold improvement of the object contrast, which is valid for all contrast objects, due to the homogeneous phantom background.

Finally, the third phantom was characterised by highly heterogeneous background (Fig. 4, third row). The background was due to the x-ray projections of consisting of a large number (more than 8 000) of various in diameter PMMA spheres, placed in water, thus creating a realistic mammography background (11,12). The enhancement of the objects' contrast in the recombined CESM image is visible for all contrast objects. The highest contrast improvement in the recombined CESM image (Fig. 4c, third row) was observed for the projected cylinder with a thickness of 0.1 mm. Although the visual enhancement of the recombined image of the heterogeneous phantom was not relatively high in comparison to the second homogeneous phantom, shown in Fig. 4, second row, still there was an enhancement for the thinner (0.1 mm) object.

Overall, the results showed that for all computer phantoms the contrast of the objects under investigation (the ROI) was higher than the contrast for low energy image. The developed phantoms could be also used in studying the correlation between quantitative assessment of contrast enhancement in CESM image and histopathology (13), whose study would be feasible due to the developed database of breast cancers by the researchers at Medical University of Varna (14).

From the studied phantoms, the third phantom, which was characterised with heterogeneous background, demonstrated production of realistic x-ray projection images and appearance of contrast inserts. This phantom is planned to be manufactured in order to validate and further use it for contrast-enhanced x-ray imaging applications. Further work also concerns the possibility to add specific detector noise to the simulated ideal x-ray images, which will contribute to the realism of the images.

## CONCLUSION

Improvement of the image quality of contrast inserts compared to low-energy x-ray images of the computational phantoms is detected for all three phantoms. The simulations with the complex com-

putational model revealed that the heterogeneous background has been successively depressed while improving the visibility of the iodine inserts. The heterogenous breast phantom might be used as a reference tool for information about the needed iodine concentration which need to be inserted during the procedure to obtain significant enhancement in the suspicious area. Current work includes the construction of the physical breast phantoms and their thorough evaluation.

***Acknowledgements:*** This research is supported by the Research Fund under grant agreement FN21021 "An Innovative Method for Quality Control of X-ray Systems".

## REFERENCES


1. Heck L, Dierolf M, Jud C, Eggl E, Thorsten S, Mechlem K, et al. Contrast-enhanced spectral mammography with a compact synchrotron source. Roeder RK, ed. PLoS ONE. 2019;14(10):e0222816. doi:10.1371/journal.pone.0222816.
2. Carton AK, Saab-Puong S, Suminski M. Seno-Bright Contrast Enhanced Spectral Mammography Technology. Published online 2012.
3. Mohamed Kamal R, Hussien Helal M, Wessam R, Mahmoud Mansour S, Godda I, Alieldin N. Contrast-enhanced spectral mammography: Impact of the qualitative morphology descriptors on the diagnosis of breast lesions. Eur J Radiology. 2015;84(6):1049-5. doi:10.1016/j.ejrad.2015.03.005.
4. Luczynska E, Niemiec J, Heinze S, Adamszyk A, Ambicka A, Marcyniuk P, et al. Intensity and pattern of enhancement on CESM: prognostic significance and its relation to expression of podoplanin in tumor stroma – a preliminary report. Anticancer Res. 2018;38(2):1085-95. doi:10.21873/anticanres.12327.
5. Mammo CESM™ Phantom (Gammex™ Technology) - Sun Nuclear. Available from: https://www.sunnuclear.com/products/mammo-cesm-phantom
6. CIRS Releases Contrast Enhanced Spectral Mammography Phantom. CIRS. Available from: https://www.cirsinc.com/news/cirs-releases-contrast-enhanced-spectral-mammography-phantom-a-simple-comprehensive-phantom-for-routine-cesm-qa/
7. Baldelli P, Bravin A, Di Maggio C, Gennaro G, Gambaccini M, Sarnelli A, et al. Evaluation of the minimum iodine concentration for contrast enhanced subtraction mammography. Nucl Instrum Methods Phys Res A. 2007;580(2):1115-8. doi:10.1016/j.nima.2007.06.109.
8. Contillo A, Taibi A. [P053] Contrast-enhanced digital mammography on commercial systems: an optimization study. Phys Med. 2018;52:114. doi:10.1016/j.ejmp.2018.06.376.
9. Bliznakova K, Speller R, Horrocks J, Liaparinos P, Kolitsi Z, Pallikarakis N. Experimental validation of a radiographic simulation code using breast phantom for X-ray imaging. Computers in Biology and Medicine. 2010;40(2):208-14. doi:10.1016/j.compbiomed.2009.11.017.
10. Bliznakova K, Buliev I, Bliznakov Z. Anthropomorphic Phantoms in Image Quality and Patient Dose Optimization: A EUTEMPE Network Book. IOP Publishing; 2018.
11. Baneva Y, Bliznakova K, Cockmartin L, Marinov S, Buliev I, Mettivier G, et al. Evaluation of a breast software model for 2D and 3D X-ray imaging studies of the breast. Phys Med. 2017;41:78-86. doi:10.1016/j.ejmp.2017.04.024.
12. Cockmartin L, Bosmans H, Bliznakova K, Pokrajac D, Imran A, Marshall N, et al. Creation of Realistic Structured Backgrounds using Adipose Compartment Models in a Test Object for Breast Imaging Performance Analysis. Published online 2016.
13. Rudnicki W, Heinze S, Niemiec J, Kojs Z, Sas-Korczynska B, Hendrick E, et al. Correlation between quantitative assessment of contrast enhancement in contrast-enhanced spectral mammography (CESM) and histopathology—preliminary results. Eur Radiol. 2019;29(11):6220-6226. doi:10.1007/s00330-019-06232-6.
14. Bliznakova K, Dukov N, Feradov F, Gospodainova G, Bliznakov Z, Russo P, et al. Development of breast lesions models database. Physica Medica. 2019;64:293-303. doi:10.1016/j.ejmp.2019.07.017.